

## Global dynamics underlying sharp basin erosion in nonlinear driven oscillators

Mohamed S. Soliman and J. M. T. Thompson

*Center for Nonlinear Dynamics and its Applications, Civil Engineering Building, University College London, Gower Street, London WC1E 6BT England, United Kingdom*

(Received 15 July 1991)

For periodically driven damped oscillators with the ability to escape from a potential well, the erosion of the nonescaping basin of attraction begins at the homoclinic tangency of the stable and unstable manifolds of the hilltop saddle cycle. The consequent *rate* of erosion, however, is intrinsically dependent upon the manifold organization, which to a large extent is determined by the heteroclinic events following the homoclinic tangency. In this paper we outline how, under small parameter changes, there can exist a rapid erosion of the nonescaping basin.

PACS number(s): 05.45.+b

### I. INTRODUCTION

In typical dynamical systems several attractors can coexist, each embedded in its own basin of attraction. Under the variation of a control parameter, as attractors move and bifurcate, the basins also undergo changes and metamorphoses; new basins are created, old basins are destroyed, and existing basins evolve [1]. Furthermore, basins of attraction can have highly intertwined or even fractal boundaries which can result in a (substantial) region of phase space having an infinitely textured homoclinic structure [2,3]. In such circumstances, with the inherent uncertainties in the specification of the initial conditions, experienced by all dynamical systems to some degree, long-term predictability can be lost [4]. Thus, from both a practical and a theoretical point of view, there has been much study concerning the qualitative and quantitative reorganization of basin structure as parameters pass through certain critical values.

Recent studies have identified and quantified how under small parameter changes, there can exist a rapid erosion and stratification of a basin, as a result of the homoclinic tangency of the stable and unstable manifolds of a regular saddle, which can have severe consequences for the integrity of an operating dynamical system [5,6]. In this paper the mechanism by which such a situation can arise is discussed. As homoclinic and heteroclinic tangencies of regular saddles play an important role in basin structure, we describe the major events that can induce conditions that lead to a sharp drop in basin area. It is shown that the erosion begins at a homoclinic tangency, but the consequent rate of erosion is largely dependant upon the manifold organization. We estimate, for a typical driven damped oscillator, parameter values that trigger this rapid erosion, and at which control values such behavior is most pronounced.

As an illustrative example, we shall consider the problem of the sinusoidally forced motions of a particle in a single potential well,  $V = \frac{1}{2}x^2 - \frac{1}{3}x^3$  [7], with the governing equation of motion

$$\ddot{x} + \beta\dot{x} + x - x^2 = F \sin \omega t,$$

where  $x$  is the dependant variable and a dot denotes differentiation with respect to time  $t$ . We define  $\dot{x} \equiv y$  and when considering Poincaré mapping, we focus attention throughout on phase  $\phi = 180^\circ$ . The positive coefficient  $\beta$  represents the magnitude of damping, and the oscillator is driven by the sinusoidal force of magnitude  $F$  and circular frequency  $\omega$ . As a specific case, chosen to illustrate the main features of basin erosion, we fix  $\omega = 0.83$  and  $\beta = 0.1$ . This value of  $\beta$  corresponds to damping ratio of  $\zeta = 0.05$  which is typical of many mechanical and physical systems.

The initial conditions will determine whether the system “escapes” to the attractor at infinity,  $x \rightarrow \infty$  as  $t \rightarrow \infty$ , or settles to a bounded oscillation as  $t \rightarrow \infty$ . In this study we consider how coexisting basins evolve as the forcing is increased through certain critical values, paying particular attention to the process of the incursive erosion by the basin of attraction of infinity (escaping basin) into the safe or bounded basin (the union of the basins of the nonescaping attractors). It has been shown that the dominant individual bounded basins of attraction belong to those attractors originating from the fundamental  $F = x = y = 0$  equilibrium state. So, generally, except during a region of resonant hysteresis, the bounded basin will be for practical purposes that of a single attractor. There are, of course, many coexisting attractors (usually with very small basins), born at saddle-node bifurcations, but these are usually observed over a small range of  $F$  before they are destroyed at a boundary crisis.

### II. OVERVIEW

Before proceeding in more detail, we give a brief and simplified overview of the mechanism of basin erosion, as shown schematically in Fig. 1, that would be common to all periodically driven nonlinear damped oscillators with the ability to escape from a potential well. The first large portrait (from the top) at low forcing  $F$  shows, in the space of the starting conditions  $\{x(0), y(0)\}$ , the gray nonescaping basin whose boundary is formed by the stable manifold (inset) of the hilltop saddle cycle,  $D_h$ . The stroboscopic Poincaré mapping point of the unique

nonresonant attractor,  $S_n$ , is shown lying in its gray basin of attraction. The constant negative divergence of flow, a consequence of the constant positive damping coefficient, implies that the basin must have infinite basin area in the full Poincare section, with a *finite* area in any finite window of interest.

The relevant bifurcational events are illustrated by the small portraits, and the first one encountered under increasing  $F$  is the saddle-node fold  $B$ , which creates a resonant saddle  $D_r$  and an adjacent resonant attracting node  $S_r$ . The negative divergence implies that  $S_r$  is born with a "residual" basin of (in)finite area.

The basin structure after the fold  $B$  is illustrated in the second large portrait. The total nonescaping basin, still bounded by the stable manifold of  $D_h$ , is now divided in two by the stable manifold of the resonant saddle,  $D_r$ . The basin of  $S_r$  is shown in black. Because the stable manifold of  $D_r$  is born heteroclinically tangled with the unstable manifold of  $D_h$ , the two bounded coexisting basins accumulate onto  $D_h$ . But the boundaries are still

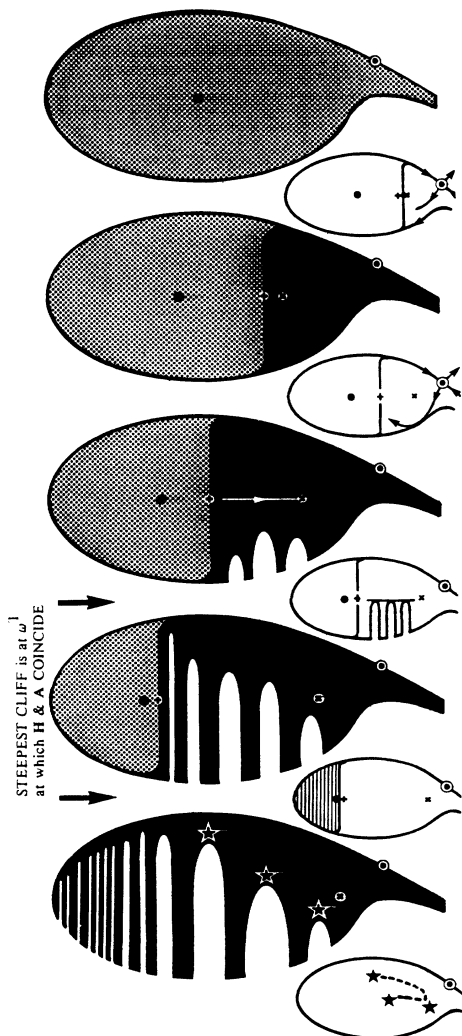


FIG. 1. Schematic representation of the mechanism of basin erosion generating a sharp loss of basin area.

smooth and as yet there is no fractal structure.

This changes at the global bifurcation  $M$  predicted accurately by a Melnikov perturbation analysis, at which the stable and unstable manifolds of  $D_h$  have a homoclinic tangency. The ensuing homoclinic tangle generates a fractal basin boundary. This situation shortly after the Melnikov tangency is shown in the third large portrait where large incursive fractal fingers are starting to penetrate into the black resonant basin. However, they have not yet crossed the white line representing the unstable manifold of  $D_r$  directed towards  $S_r$ , and the rate of erosion of the safe basin, comprising the union of the basins of  $S_r$  and  $S_n$ , is still relatively low.

However, when there is a heteroclinic tangency  $H$  at which the stable manifold of  $D_h$  touches the unstable manifold of  $D_r$ , there is a triggering of a major fractal incursion in which the escaping fractal fingers flash through the unstable manifold of  $D_r$  and accumulate on the stable manifold of  $D_r$ . This generates the rapid rate of erosion of the safe area, under increasing  $F$ , at fixed value of  $\omega$ .

Since its creation with  $S_r$  at fold  $B$ , the resonant saddle  $D_r$  has been moving steadily across the portrait towards  $S_n$ , and at fold  $A$  we witness their collision and annihilation. This marks the end of the hysteresis regime involving the two major coexisting harmonic attractors,  $S_r$  and  $S_n$ . At this fold  $A$ , the (in)finite residual basin of  $S_n$  is instantaneously infinitely striated. Under further increase of  $F$ , these fine striations thicken out, so that in the final portrait the whole of the black basin of  $S_r$  is heavily eroded by relatively thick fingers. The erosion process continues as a sequence of basin implosions associated with short-lived subharmonic cascades at the extremities of the major incursive fingers and related changes in accessible saddle orbits.

Meanwhile, the resonant harmonic attractor,  $S_r$ , period-doubles to a chaotic attractor which is annihilated in a final collision with the current accessible orbit. This boundary crisis,  $E$ , marks the end of the main sequence of attractors after which there is no (major) attractor available to the system and (almost) all the transients lead to escape. There may indeed be small regimes of  $F$  containing bounded attractors but these usually have very small basins of attraction.

### III. CONDITIONS LEADING TO A DRAMATIC EROSION OF THE BASIN OF ATTRACTION

Having briefly described the main events concerning the basin-erosion process, we now look in more detail at the role of the stable and unstable manifolds of the main regular saddles, which to a large extent, determine the properties of basins of attraction. For systems with the ability to escape out of a potential well, the hilltop saddle cycle  $D_h$ , which originates from the unstable equilibrium  $\{F=y=0, x=1\}$ , plays a key role. It is the stable manifold  $W^s(D_h)$ , of  $D_h$ , which consists of two components either side of the saddle, that defines the boundary between the escaping and nonescaping (safe) basins. For relatively small forcing levels, the basin boundary is smooth; initial points starting outside this boundary map under forward

time to the attractor at infinity, whereas points within it map to a small stable  $n=1$  oscillation  $S_n$ , which originates from the stable equilibrium position  $\{F=x=y=0\}$ . The unstable manifold of  $D_h$ ,  $W^u(D_h)$ , also has two components. The left-hand interior (within the potential well) branch,  $W^u_A(D_h)$  lies completely within the basin of  $S_n$ , with points on it mapping to  $S_n$  as  $t \rightarrow \infty$ . The right-hand exterior branch  $W^u_B(D_h)$  lies completely outside the safe basin, points on it mapping towards the attractor at infinity.

As the forcing is increased, the system approaches a saddle-node bifurcation (at  $F^B = 0.0488$ ), which will result in a new saddle-node pair  $D_r$  and  $S_r$  ( $r$  for resonant,  $n$  for nonresonant). Accordingly, although there is no change in topological structure before  $F^B$ , there is considerable underlying manifold reorganization associated with the impending accumulations; most significant is the increased distortion of  $W^u_A(D_h)$  in the neighborhood of the imminent saddle-node creation of an  $S_r$  basin [8].

At the saddle-node bifurcation at  $F^B$ , there is the instantaneous creation of a basin for  $S_r$ , within the safe nonescaping basin still bounded by  $W^s(D_h)$ . It follows from the continuous contraction of phase area, and the corresponding increase of area under negative time, that the basin is born with infinite area in the full Poincaré section. Within a finite window of this section, it will be born with a finite nonzero area, implying an instantaneous equal and opposite decrease in the area of the basin of  $S_n$ .

Figure 2(a) shows the invariant manifolds [9], shortly after the saddle-node bifurcation, where the node has moved away from the saddle into the interior of its basin. The boundary between the  $S_n$  and  $S_r$  basins is  $W^s(D_r)$ , both branches of which tend to  $x = +\infty, y = -\infty$ , as  $t \rightarrow -\infty$ . Both branches are born heteroclinically tangled with  $W^u_A(D_h)$  so that simultaneously with the saddle node at  $F^B$ , we have the two heteroclinic conditions,  $het(1); W^u_A(D_h) \cap W^s_A(D_r) \neq \emptyset$ , and  $het(2); W^u_A(D_h) \cap W^s_B(D_r) \neq \emptyset$ .

It follows firstly that  $W^u_A(D_h)$  is accumulated on either side of  $W^u(D_r) \equiv W^u_A(D_r) \cup W^u_B(D_r)$ , the unstable manifold of  $D_r$ , so that  $W^u(D_r)$  is contained within the closure of  $W^u_A(D_h)$ ; this results in the manifold exhibiting a *banded* structure in this region. Secondly,  $W^s_A(D_r)$  and  $W^s_B(D_r)$  are accumulated on the "inside" of the global basin boundary formed by  $W^s(D_h)$ , so that  $W^s(D_h)$  is contained within the closure of  $W^s(D_r)$ . There is thus a

crossing the unstable manifold will, under negative time, be drawn towards the saddle and contract in width by approximately  $1/\Lambda_U \approx 0.00088$ , and be stretched by  $1/\Lambda_S \approx 2440$ , i.e. *very* fast stretching and contraction occurs near the saddle. This explains why "tails" of the  $S_r$  basin accumulating onto the stable manifold of  $D_h$  are not visible near  $D_h$ . On the other hand, at these parameter values, the eigenvalues of the resonant saddle,  $D_r$ , are  $\Lambda_S \approx 0.351$  and  $\Lambda_U \approx 1.337$ , implying that, here the contraction and stretching actions are less pronounced as observed by the accumulation of  $W^u_A(D_h)$  onto  $W^u(D_r)$ .

As the forcing is further increased, a continuous reorganization between the two competing bounded basins takes place and  $W^s_A(D_h)$  approaches  $W^u_A(D_h)$  until they touch at a homoclinic tangency at  $F^M = 0.0623$ , which has been predicted accurately for the  $\omega$  values of current interest, by a Melnikov analysis [7,10]. One tangency of the manifolds implies an infinite number of tangencies, and at  $F^M$  we shall observe  $W^s_A(D_h)$  accumulating on  $W^s_B(D_h)$  and  $W^u_A(D_h)$  accumulating on itself. An infinite number of fingers of the unsafe basin bounded by  $W^s_A(D_h)$  will thus be lined up roughly parallel to  $W^s_B(D_h)$ , all fingers touching  $W^u_A(D_h)$  at  $F^M$ .

The homoclinic tangling can be written as  $hom(1): W^u_A(D_h) \cap W^s_A(D_h) \equiv \emptyset$ , after the tangency  $W^s_A(D_h)$  accumulates on *both*  $W^s_A(D_h)$  and  $W^s_B(D_h)$ . The infinite series of progressively longer and thinner fingers now accumulate on the inside of the stable manifold  $W^s(D_h)$ , giving the well-known fractal basin boundary [2]. In the terminology of Grebogi *et al.* [11], the hilltop saddle cycle  $D_h$  is now inaccessible from the finite attractor but is still accessible from the attractor at infinity. The infinity of fingers of the fractal boundary is a manifestation of escaping chaotic transients, of arbitrary duration, associated with the mapping from one finger to the next.

Figure 2(b) illustrates, at a forcing level above that of the homoclinic tangency, the initial development of the tangling process. Here the tip of the main finger, area  $R^0$ , maps to the smaller area  $R^1$  under one forcing period, which in turn maps to smaller and smaller fingers  $R^2, R^3, \dots$  accumulating along  $W^u_B(D_h)$ ; however, due to earlier considerations concerning the dynamics close to  $D_h$ , we may say most points mapping from area  $R^0$  tend *very* quickly to large  $+x$  and  $+y$ . Here it must be noted that although the eigenvalues of the hilltop and resonant saddles have, of course, changed, their orders of magnitude remain roughly the same.

relative contraction and stretching actions in different parts of the phase space,  $R^{-1}$  has very thin “tail” passing very close to the left of  $D_h$  following the *initial* path of  $W_A^s(D_h)$ , but has a more visible “head” due to the actions of the resonant saddle. The earlier finger  $R^{-2}, R^{-3}, \dots$  are not visible, but constitute progressively longer and thinner fingers which wrap around the shorter fatter fingers. However, at this stage, this highly intertwined fractal structure is confined as a thin layer which is highly compressed against the outer edge of the basin boundary.

As the forcing is further increased, the erosion contin-

ues; Fig. 2(c) shows the development of the tangle. The main finger  $R^0$  makes *further* intersections with  $W_A^u(D_h)$ , corresponding to important changes in Birkhoff signature [12,13]. All forward and backward images  $R^i$ , make corresponding synchronized further intersection, with more fingers moving up into the bounded basin. Such behavior can clearly be seen in this figure where three preimages of  $R^0$  are clearly visible.

Additional homoclinic and heteroclinic connections occur, which have significance for both the basin structure and the forthcoming saddle-node annihilation of  $S_n$  and  $D_r$  [8]. Firstly, there is a homoclinic tangling of

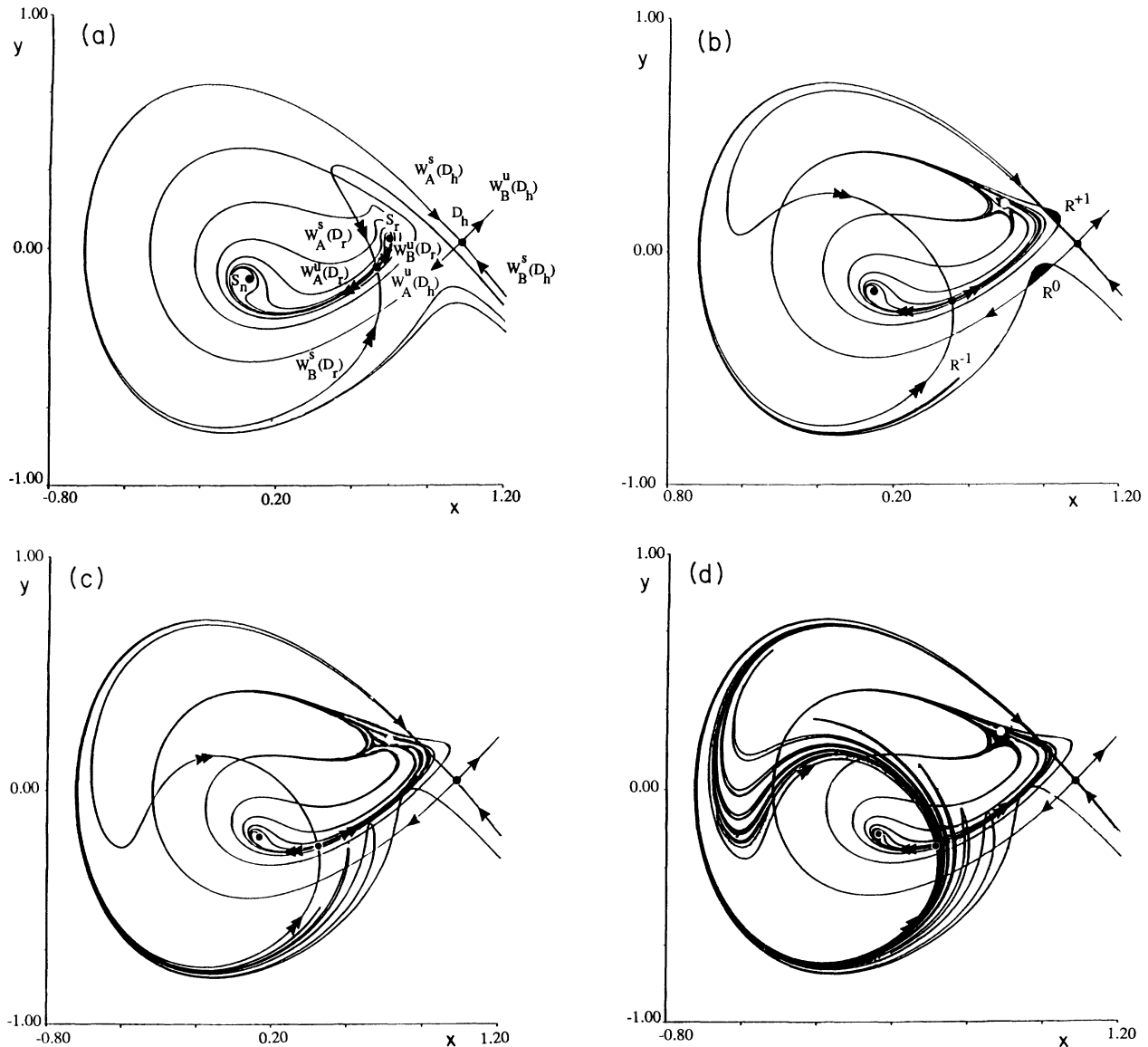


FIG. 2. (a) Manifold organization at  $F=0.05$ ; just after the saddle-node creation, there is an accumulation of  $W_A^u(D_h)$  onto  $W^u(D_r)$  and an accumulation of  $W^s(D_r)$  onto  $W^s(D_h)$ . Also the “knee” of  $W_A^s(D_h)$  moves towards  $W_A^u(D_h)$  as a homoclinic tangency is approached. (b) Manifold organization at  $F=0.065$ ; after the homoclinic tangency, at  $F^M=0.0623$ , the basin boundary has become *fractal*, resulting in the incursion of the safe basin by fingerlike projections. (c) Manifold organization at  $F=0.070$ ; here we can see the imminent homoclinic tangling of  $W_B^u(D_r)$  with  $W_A^s(D_r)$ . (d) Manifold organization at  $F=0.071$ ; the manifolds and basins after het(3) are shown, clearly illustrating the accumulation of the escaping fingers, from the right-hand side of the saddle  $D_r$ , onto the stable manifold  $W^s(D_r)$ .

$W_B^u(D_r)$  with  $W_A^s(D_r)$ , hom(2):  $W_B^u(D_r) \cap W_A^s(D_r) \neq \emptyset$ , which is closely followed by hom(3):  $W_B^u(D_r) \cap W_B^s(D_r) \neq \emptyset$ , resulting in fingers of  $W^s(D_r)$  accumulating around  $D_r$ .

More important, however, is the heteroclinic event het(3):  $W_B^u(D_r) \cap W_A^s(D_h) \neq \emptyset$  which involves the basin boundary of the attractor at infinity. As this heteroclinic tangency is approached, fingers  $R^i$  of  $W_A^s(D_h)$  approach  $W_B^u(D_r)$ , onto which is accumulated  $W_A^u(D_h)$ , resulting in a rapid cascade of Birkhoff signature changes associated with higher-order crossings of  $W_A^s(D_h)$  and  $W_A^u(D_h)$ . At the heteroclinic tangency, there will be an infinite number of escaping fingers lined up along  $W_B^u(D_r)$  and after the tangency,  $W_A^s(D_h)$  accumulates on both  $W_A^s(D_r)$  and  $W_B^s(D_r)$  [Fig. 2(d)].

Unlike the smooth-fractal transition at hom(1), where the penetration of the escaping fingers was limited to the periphery of the bounded basin, here the event is truly incursive. The relatively slow mappings in the central region of phase space, as well as the action of the resonant saddle, have important geometrical implications for the basin structure. As preimages of  $R^0$  increase in area under negative iteration by  $e^{2\pi\beta/\omega} = \Lambda_S \Lambda_U$ , a small increase of forcing, which results in a small increase in area of  $R^0$ , can induce a relatively large increase in the areas of  $R^{-1}, R^{-2}, R^{-3}, \dots$  in the region considered. More and more visible escaping fingers, under a relatively small change in  $F$ , can quickly grow in size, then penetrate and disintegrate the bounded basin. This is clearly seen in Fig. 3, where fingers accumulate firstly on  $D_h$ , grow in size, wrap around  $D_r$ , and then again are quickly stretched near  $D_h$ . Longer thinner fingers which wrap around the shorter fatter fingers repeat this scenario over and over.

Integrity measures, which quantify how the basins of attraction change in size in both the local and the global sense, may be used to assess such behavior [5,14]. Figure 4 shows the variation of basin area (global integrity), within a given window of initial conditions, plotted against  $F$ . Here it can clearly be seen that there is no significant change of total basin area up to  $F^B$ , where upon there is a finite jump in area of the  $S_r$  basin, which results in an equal and opposite drop in area of the  $S_n$  basin. As the forcing is increased, there is no macroscopic change in the total area but there is a natural interchange between the two competing basins. This process continues up to the Melnikov tangency at  $F^M$ , resulting in the initial incursion by the escaping fingers and hence a small decrease in area; at  $F^H$ , these fingers then become truly incursive and invade the center of the basin, giving the clifflike reduction in area. The basin continues to be eroded, at various rates, as new basins are born (e.g.,  $S^3$  basin at  $F=0.079$ ) and old basins die (e.g.,  $S_n$  basin at  $F=0.08$ ). The effects of the resonant saddle, with its associated accumulations, still remain after its destruction at a saddle-node annihilation. The erosion continues until the final escape at a boundary crisis at  $F^E=0.095$ . It can be seen that there are metastable transient basins after this event, associated with the folding in phase space [15]. These results show that although the homo-

clinic tangency hom(1) triggers the beginning of the incursive erosion of the bounded basins, it is the heteroclinic event het(3), or its virtual derivatives, that signifies the dramatic erosion of basin area.

IV. GLOBAL VIEW OF BASIN EROSION

Having identified the main bifurcations and events that can induce a sharp drop in basin area, we briefly put these results in a wider context, as presented in the bifurcation diagram in  $(F, \omega)$  control space, in the locality of the primary resonance, in Fig. 5. Lines A and B are saddle-node folds corresponding to jumps to and from resonance. Line C is the first period-doubling flip bifurcation, at which the resonant harmonic attractor period-doubles to a stable subharmonic of order 2. There is an infinite cascade of these flip bifurcations leading to a chaotic attractor which finally loses its stability at a crisis at E. Line M is the locus of the homoclinic tangency of  $W_A^s(D_h)$  and  $W_A^u(D_h)$ . Line H is the heteroclinic tangency het(3), between  $W_A^s(D_h)$  and  $W_B^u(D_r)$ , which generates

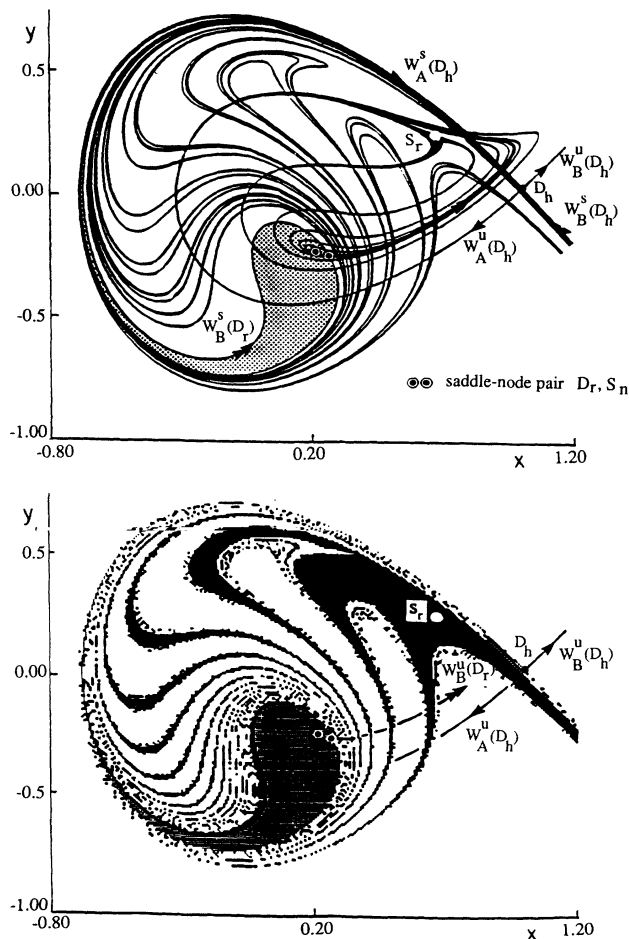


FIG. 3.  $F=0.0795$ ; the manifolds (upper panel) and the basins of attraction (lower panel) just before the tangled saddle-node bifurcation at  $F^A=0.080$ , showing the mass erosion of the resonant basin of attraction.

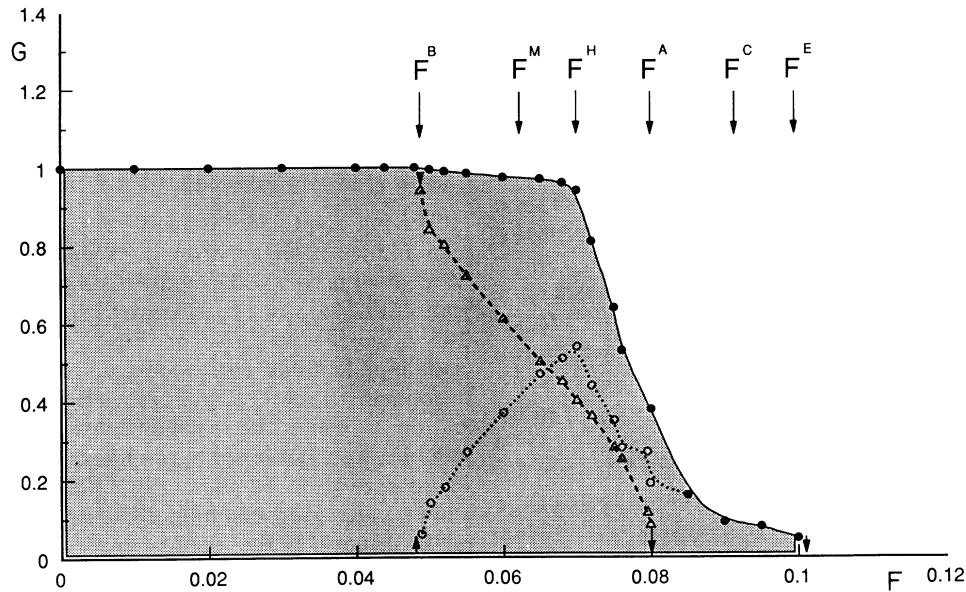


FIG. 4. The normalized (with respect to the safe basin area at  $F=0$ ) area of the safe basin,  $G$ , within the window of initial conditions  $-1.2 < x < 0.8$ ,  $-1.0 < y < 1.0$ , is plotted against the forcing magnitude  $F$ . Here  $\omega$  is fixed at 0.83. The solid line represents the total basin area; the dashed line represents the basin area of the nonresonant attractor; and the dotted line represents the basin area of the resonant attractor.  $F^M$  is forcing level in which there is a homoclinic tangling,  $\text{hom}(1)$ , and  $F^H$  is where there is a heteroclinic tangling  $\text{het}(3)$ .

an indeterminate jump to resonance at the saddle node  $A$  above  $T$  [8,16]. We have also extrapolated line  $H$ , as shown by the dashed line  $h$ . Although for these parameter values there is no heteroclinic event (for the simple reason that  $D_r$  does not exist to the right of arc  $A$ ) we might say that, due to dynamical continuity, there is a “virtual” heteroclinic event, signifying the impending sharp drop in resonant basin area. The type of dynamical continuity we have in mind here concerns the average rate of flow of trajectories in a macroscopic region of phase space, a quantity (unlike the qualitative topological form of attractors and basins) that will be preserved across any bifurcation boundaries in control space. We have also drawn contours of constant global integrity (constant basin area) and we can see that the arc  $H$ - $h$  correlates well with the top of the sharp cliff, identifiable by the closely spaced contours. These have important implications for systems operating in essentially transient conditions [17].

For frequencies below  $\omega^T$ , the bounded basin will primarily consist of two parts: the nonresonant  $S_n$  basin and the corresponding resonant  $S_r$  basin. Under increasing  $F$ , fold  $B$  signifies the birth of the  $S_r$  basin, and consequently the beginning of the interchange, as is usual in a region of resonant hysteresis, of the  $S_n$  basin into the  $S_r$  basin. For forcing levels just above  $F^M$ , there is the initial incursion of the bounded basin by the escaping basin, while  $F^H$  signifies the beginning of the mass erosion of the  $S_r$  basin. For systems where the union of the non-escaping basins is of interest (i.e., the total bounded basin), the nonresonant basin seems to “shore up” the bounded basin.

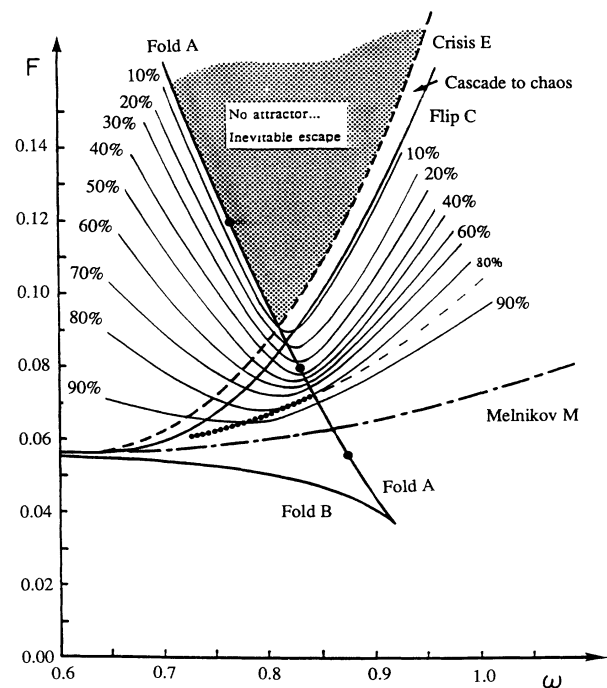


FIG. 5. Bifurcation diagram in the  $(F, \omega)$  control space at  $\beta=0.10$ . The dotted line indicates the heteroclinic tangency  $H$  between the unstable manifold  $W_B^u(D_r)$  of the resonant saddle and the stable manifold  $W_A^s(D_h)$  of the hilltop saddle; the extrapolation  $h$  of this line is indicated by the dashed line. The intersection of line  $H$  with line  $A$  corresponds to point  $T$ . The intersection of line  $E$  with line  $A$  corresponds to point  $Q$ . Also shown are contours of constant integrity (constant basin area).

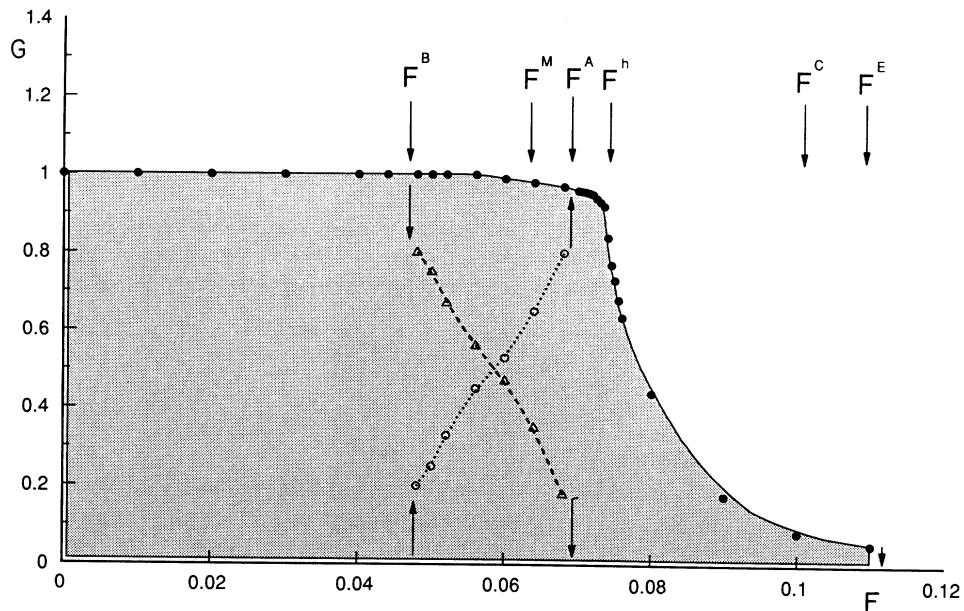


FIG. 6. Same details as Fig. 4, but here  $\omega$  is fixed at 0.85.  $F^h$  represents the forcing level at which there is a “virtual” heteroclinic tangling,  $\text{het}(3)$ .

For frequencies above  $\omega^T$ , a similar erosion process takes place, but here most of excursive interchanges between the resonant and nonresonant basins will have taken place before  $h$ . This implies that for these parameter values the mass erosion of the basins, predicted by  $h$ , will seem more pronounced, as the erosion will take place throughout the *whole* of the bounded basin, rather than just part of it. This is clearly seen in Fig. 6 at  $\omega=0.85$ . These results, as the contours of constant integrity confirm, imply that  $\omega^T$  is a critical frequency for this nonlinear dynamical system, as it corresponds to the value at which the basin area is likely to be eroded most rapidly under increased forcing.

In conclusion basin erosion has been shown to be a typ-

ical feature of a wide class of nonlinear oscillators preceding optimal or near-optimal escape [5,17,18]. We described the mechanism of basin erosion and identified the main basin bifurcations involved in this process. This gives us a greater understanding when defining a criterion of integrity for a physical system operating in a noisy or ill-defined environment [6].

#### ACKNOWLEDGMENT

The authors would like to thank the Science and Engineering Research Council of the United Kingdom, which made this work possible.

- [1] E. Eschenazi, H. G. Solari, and R. Gilmore, *Phys. Rev. A* **39**, 2609 [1989].  
 [2] S. W. McDonald, C. Grebogi, E. Ott, and J. A. Yorke, *Physica D* **17**, 125 (1985).  
 [3] F. C. Moon and G. X. Li, *Phys. Rev.* **55**, 1439 (1985).  
 [4] C. Grebogi, S. W. McDonald, E. Ott, and J. A. Yorke, *Phys. Lett. A* **99**, 415 (1983).  
 [5] M. S. Soliman and J. M. T. Thompson, *J. Sound Vib.* **137**,

- [11] C. Grebogi, E. Ott, and J. A. Yorke, *Physica D* **24**, 243 (1987).  
 [12] R. H. Abraham and C. D. Shaw, *Dynamics: The Geometry of Behaviour, Part III, Global Behaviour* (Ariel, Santa Cruz, CA, 1985).  
 [13] F. A. McRobie and J. M. T. Thompson, *Proc. R. Soc. London Ser. A* **435**, 659 (1991).  
 [14] M. S. Soliman and J. M. T. Thompson, *J. Sound Vib.* **137**,

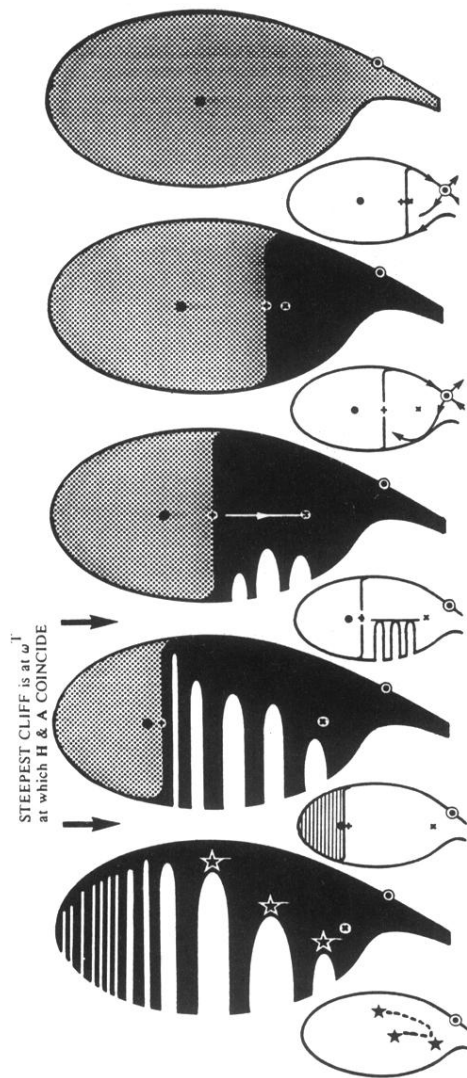


FIG. 1. Schematic representation of the mechanism of basin erosion generating a sharp loss of basin area.

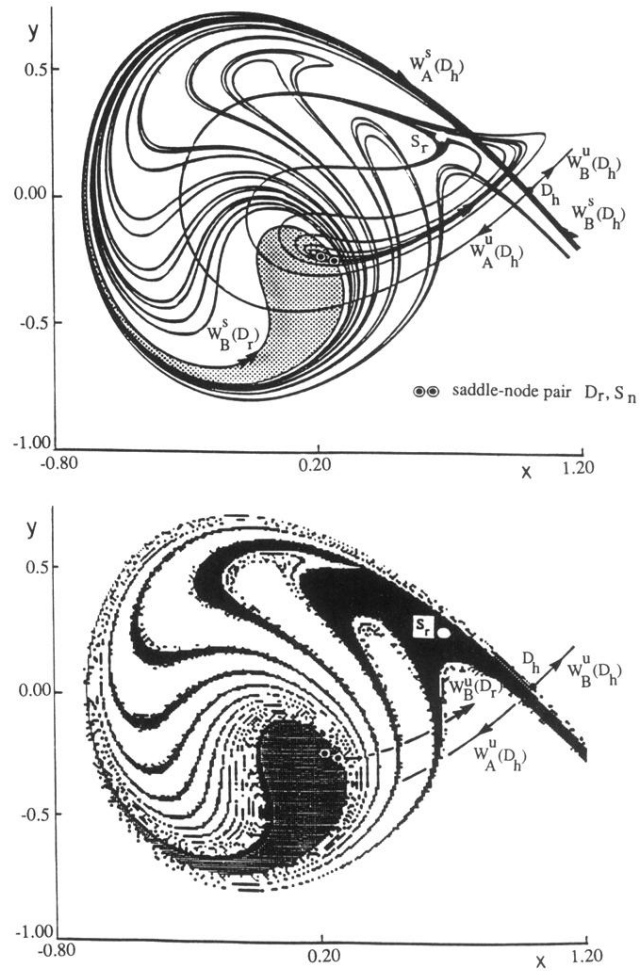


FIG. 3.  $F=0.0795$ ; the manifolds (upper panel) and the basins of attraction (lower panel) just before the tangled saddle-node bifurcation at  $F^A=0.080$ , showing the mass erosion of the resonant basin of attraction.

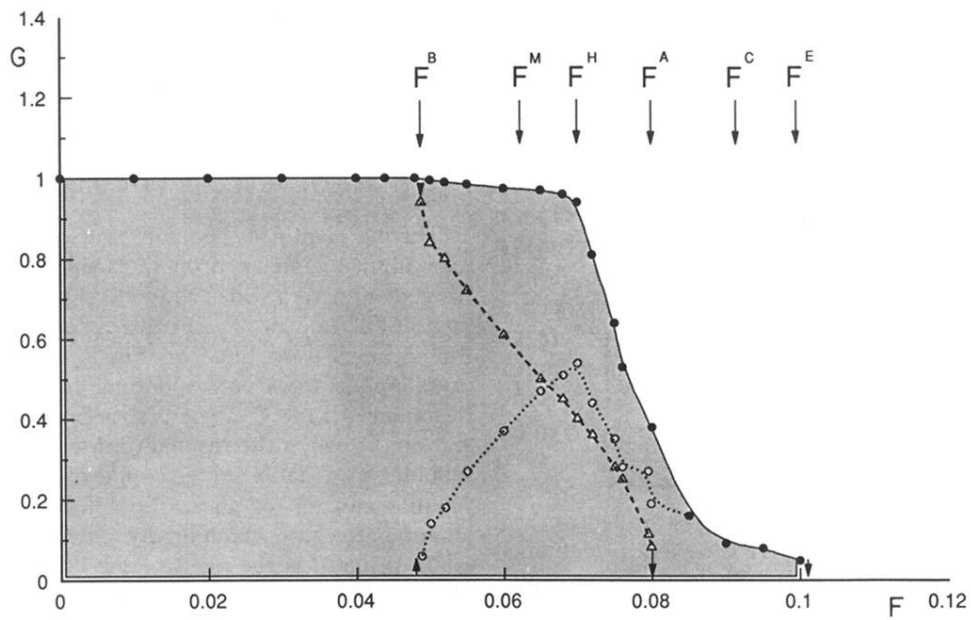


FIG. 4. The normalized (with respect to the safe basin area at  $F=0$ ) area of the safe basin,  $G$ , within the window of initial conditions  $-1.2 < x < 0.8$ ,  $-1.0 < y < 1.0$ , is plotted against the forcing magnitude  $F$ . Here  $\omega$  is fixed at 0.83. The solid line represents the total basin area; the dashed line represents the basin area of the nonresonant attractor; and the dotted line represents the basin area of the resonant attractor.  $F^M$  is forcing level in which there is a homoclinic tangling,  $\text{hom}(1)$ , and  $F^H$  is where there is a heteroclinic tangling  $\text{het}(3)$ .

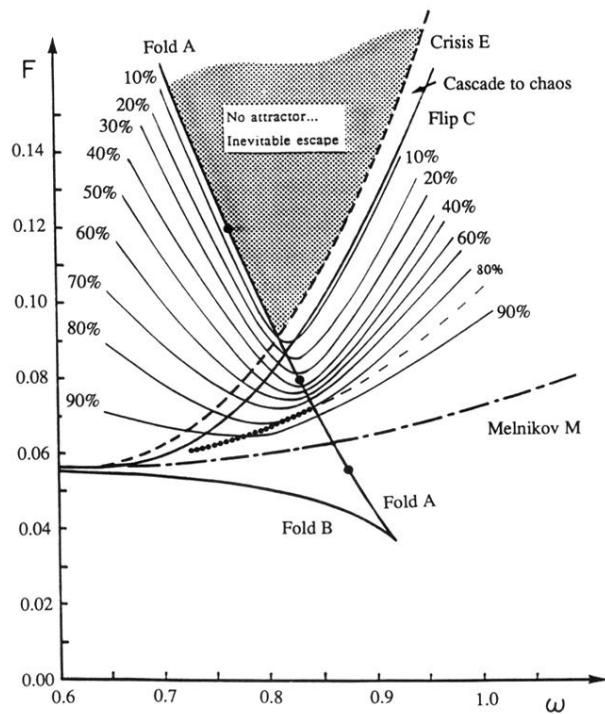


FIG. 5. Bifurcation diagram in the  $(F, \omega)$  control space at  $\beta=0.10$ . The dotted line indicates the heteroclinic tangency  $H$  between the unstable manifold  $W_B^u(D_r)$  of the resonant saddle and the stable manifold  $W_A^s(D_h)$  of the hilltop saddle; the extrapolation  $h$  of this line is indicated by the dashed line. The intersection of line  $H$  with line  $A$  corresponds to point  $T$ . The intersection of line  $E$  with line  $A$  corresponds to point  $Q$ . Also shown are contours of constant integrity (constant basin area).

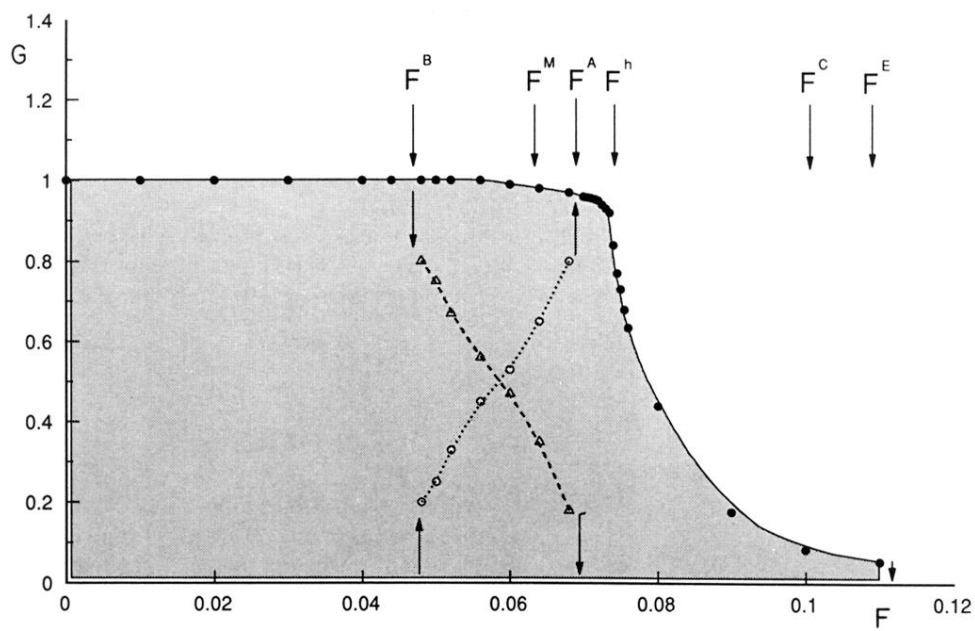


FIG. 6. Same details as Fig. 4, but here  $\omega$  is fixed at 0.85.  $F^h$  represents the forcing level at which there is a “virtual” heteroclinic tangling,  $\text{het}(3)$ .